Analyst

Accepted Manuscript

ROYAL SOCIETY OF CHEMISTRY

www.rsc.org/analyst

Journal Name RSCPublishing

ARTICLE

Raman microspectroscopy of human aortic valves: investigation of local and global biochemical changes associated with calcification in the aortic stenosis

Cite this: DOI: 10.1039/x0xx00000x

Received 00th January 2012,
Accepted 00th January 2012

DOI: 10.1039/x0xx00000x

www.rsc.org/

Krzysztof Czamara,[a,b] Joanna Natorska,[c] Przemysław Kapusta,[d] Malgorzata Baranska[a,b] and Agnieszka Kaczor[a,b*]

Raman microimaging has been applied to study of the biochemical composition in the aortic valves obtained from patients with calcified aortic stenosis. Aortic stenosis affects an increasing number of elderly patients with hyperlipidemia and hypercholesterolemia. Lipids accumulation in the tissue is associated with pathogenesis and progression of cardiac valve calcification. It is in line with our finding that lipid deposits, predominantly made of cholesterol and its esters, are frequently co-localized with calcium salt deposits, even at an early stage of its development. Overall changes in the biochemical composition of the tissue upon pathology progression are less obvious. Globally, although the cholesterol level rises, the relative lipid-to-protein content decreases. The results broaden the knowledge about the biochemical alterations in dysfunctional human aortic valves and may be helpful in designing of lipid lowering therapies.

Introduction

The aortic valve is a fluidic control component that maintains directionality in the blood flow from a left ventricle to the aorta during the cardiac cycle. It is situated in the root of aorta and in the normal aortic valve is consisting of three cusps.[1] Histologically, each cusp is well-defined with distinct tissue layers: the *fibrosa,* proximal to the aorta, composed mainly of collagen fibers, the *ventricularis* from the ventricular side, containing collagen together with elastin, and the *spongiosa*, a layer between the fibrosa and ventricularis, rich in proteoglycans and glycosaminoglycans.[2–4] Additionally, the valve leaflet is covered by the layer of endothelium functioning as a barrier between the blood and inner part of the cusp and playing an active role in regulatory processes i.e. by releasing nitric oxide (NO).[5,6]

The main function of the aortic valve is related to its biomechanical properties. This flap-like structure opens and closes about 3 billion times over a period of 70 years of human life.[2] The mechanical damage in the valve tissue is the origin of a subsequent disease outbreak. Calcific aortic valve stenosis (AS) is a slowly progressive disease characterized by thickening of valve cusps, fibrosis and calcification of the tissue.[7,8] AS is one of the most common heart valve diseases in the Western world developing in 2-3% of the population by the age of 65 years.[9] On average, 50 000 aortic valve replacements are performed both in Europe and the United States every year.[10] Several lines of evidence indicate that AS shares clinical and histological similarities with the active pathobiology of atherosclerosis.[11] Thus, risk factors involved in the atherosclerosis development and progression, including the elevated level of serum LDL cholesterol and lipoprotein(a), hypertension, smoking, diabetes mellitus, and male sex could function in AS.[12,13] Nevertheless, it is thought that the most significant factors are those connected with a high concentration of lipids, especially hyperlipidemia and hypercholesterolemia.[13] In the first step of aortic stenosis, endothelial injury occurs[14] enabling lipids to penetrate within the valves tissue and to accumulate in the valvular fibrosa layer.[15] Thus, the aortic valve endothelium activates and abnormal oxidation states.[13] The low-density lipid (LDL) cholesterol and its oxidation products can stimulate local inflammation and accelerate cell proliferation and bone matrix production.[16] Additionally, lipid clusters may serve as niduses for mineralization.[17] This findings led to generalization that accumulation of lipids is associated with the pathogenesis and progression of cardiac valve calcification.[18] A calcific process of valve leaflets has also many features similar to bone formation that is manifested among other by the expression of osteopontin.[19,20]

Raman spectroscopy (RS) is a non-destructive and label-free method providing fast information about the molecular

structure of a studied sample, therefore it is increasingly used to investigate samples of a biological origin.[21–27] Particularly interesting and non-trivial topic is the use of RS in the analysis of biochemical changes of animal cells and tissues upon progression of various pathologies.[28–32]

In our previous experiments we used Raman microimaging to investigate the inorganic deposits in the tissue, describing the chemical structure, distribution, size and shape of calcium phosphate inclusions in stenotic aortic valves.[33] The aim of this study was to determine the biochemical alterations of the tissue in stenotic aortic valves, particularly in the vicinity of inorganic salts.

Experimental

Sample preparation

Stenotic aortic valves were obtained from patients with severe AS undergoing elective valve replacement surgery. Patients gave their informed written consent and the study was approved by the Bioethical Committee for the Jagiellonian University. A total number of 17 stenotic and 4 control human aortic valves were studied. Control aortic valves were obtained at autopsy from age-matched apparently healthy subjects, without morphological valvular or other cardiac disorders. Stenotic ones was selected according to scoring system 0, 1, 2: no calcium nodules, isolated calcium nodules and abundant calcification, respectively. The cusps and/or cusps fragments with isolated calcium nodules were subjected into the analysis. The specimens were embedded in tissue cryopreservation medium (Tissue Tek-O.C.T. compound, Sakura Finetek USA, Torrance, California) and frozen. For Raman measurements, the they were positioned in the cryostat chamber (Leica Jung CM 3000), cut into sections with a thickness of 5-8 µm and placed on CaF_2 slides (25×2mm, Pike Technologies, U.S.). Sections were taken transversely from the mid of the leaflet and from commissural areas. Sections were fixed with ethanol/acetone (11 samples) or air dried (10 samples including all controls). For examination of valve biochemistry only the last ones were chosen to avoid the influence of fixation on degradation of proteins and lipids leaching.

Additionally, ten transverse sections (3 and 7 for control and AS, respectively) were taken from the mid and commissural areas of the leaflet and stored at –20ºC until staining. Sudan III (orange) was used to stain lipids within aortic valves. Sudan III staining was performed for 10 minutes, washed out with distilled water, and counterstained with Mayer's hematoxyline for 4 minutes. Sections were viewed in fluorescent microscope (Nikon Eclipse i50, Japan). Photomicrographs were taken using a Moticam Pro 282 camera and analyzed using image analysis software.

Spectroscopic imaging and data analysis

Raman data were collected using a confocal Raman microscope WITec Alpha 300 equipped with a CCD detector (Andor, DU 401-BV), a 600/mm grating, and an 100x air objective (Olympus MPLAN, NA=0.90). Spectra were recorded with the air cooled solid state laser with the excitation line of 532 nm. The measurement parameters were optimized and for all samples the integration time of 0.3 s, the laser power of about 5 mW and spectral resolution of 3 cm^{-1} were used. Raman spectra were acquired for areas of various sizes from 5.0x10.3 µm to maximally 13.7x21.6 µm. All spectra were measured with the 0.12 µm step in the x/y plane resulting in the lateral resolution of 0.36 µm. Raman measurements were performed mainly at the aortic side of the valve according to the general knowledge about the disease progression in calcific aortic stenosis. For each valve spectra from at least two Raman areas were measured that resulted in a total of 39 hyperspectral data sets.

All spectral data processing including baseline correction (polynomial of degree 2), cosmic rays removal and Cluster Analysis (CA, Manhattan distance), was performed using WITec Project Plus software. The aim of CA is to group spectra from the acquired datasets into classes, in which spectra have the most similar spectral features.[34,35] According to a defined distance measure, the differences between the data within each class are minimized and the differences between classes are maximized. Thus, the large amount of spectra is reduced to mean spectra of classes. Average spectra for control and stenotic valves were processed in OPUS program.

Results and discussion

Chemical profile of stenotic and control aortic valves

Lipids

An increased lipid content in tissues and cells is in many cases considered a condition of disease progression, for instance in atherosclerosis, liver steatosis or diabetes.[28,29,36] The local lipid accumulation associated with calcification was noticed also in stenotic valves. Lipid features in Raman spectra are easy to observe due to the large Raman scattering cross-section of lipid signals. Additionally, based on the characteristic marker bands of different groups of lipids, various lipids can be identified.[37,38] Fig. 1 shows the average Raman spectra extracted from Raman images of the aortic valve tissue. The first one (Fig. 1A) is a representative spectrum originating from an image with the high concentration of lipids.

A representative lipid spectral profile in the valve tissue (A) is manifested mostly by the bands at 1444 and 1304 cm^{-1}, originating from the CH_2 scissoring and twisting modes, respectively. A quite intense band at 1670 cm^{-1} indicates the presence of the C=C bonds. The unsaturation of alkyl chains is revealed also as the features characteristic for the deformations and stretching vibrations of the =C-H moiety that are observed at 1271 and 3014 cm^{-1}, respectively. In the fingerprint region also three characteristic bands of the sterol ring deformations are observed at 428, 548 and 704 cm^{-1}, respectively.[37] The band at 1740 cm^{-1}, related to the C=O stretching vibrations, is also present. Its position varies depending on the type of the lipid and in this case is assigned to cholesteryl esters.[37] Both the

above-mentioned bands and the overall shape of the spectrum indicate the presence of cholesterol and its derivatives in the tissue. In fact cholesterol and its esters are the most predominant lipid features in the average spectra of both high-lipid areas and also areas rich in calcium salts (B). Also the features at 428, 548 and 704 cm^{-1}, unique for cholesterol and its esters, are clearly seen in the average spectra of stenotic valves (C).

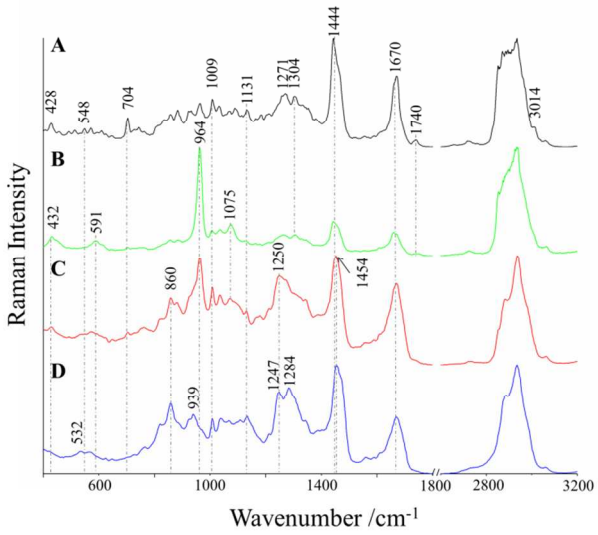

Fig.1. The average Raman spectra of the dataset recorded from the area of the stenotic valve with high concentration of lipids (A) or calcium salts (B) and the spectra of stenotic (C) and control (D) valves averaged over all measurements. Both spectral ranges were maximally extended in the y-axis.

Fig. 1C and 1D show the comparison of the average spectra of stenotic and healthy valves, respectively. Both were averaged over all measurements. The average spectrum of the stenotic valves reveals typical Raman features assigned to lipids, proteins and calcium salts. The main spectral features with their assignment are listed in Table 1. Apart from the presence of calcium salts in the spectra of stenotic valves (described below), the utmost changes are observed in the amide III region. Two well resolved bands at 1247 and 1284 cm^{-1} are observed for the control valves, contrarily to the pathological valves, where the lower-wavenumber component is dominating. Other distinctive bands of different relative intensity in the analyzed spectra are at 860 cm^{-1} at 939 cm^{-1}, possibly originating from the C-C stretching vibrations of proline present in collagen, and at 1009 cm^{-1}, assigned to phenylalanine.

To investigate statistically the global information about lipid changes in the tissue upon AS development, intensity ratios of characteristic bands due to lipids and proteins were determined (Fig. 2). Fig. 2 presents ratios of the integral intensity of key bands due to lipids and proteins in the analyzed samples.

Table 1. Assignment of bands in the Raman spectra of human aortic valves.

Band wavenumber /cm^{-1}	Assignment		
	Calcium salts	Lipids	Proteins
3014		ν_{as}(=C-H)[46]	
2830-2960		$\nu(CH_2/CH_3)$[46]	
1740		ν(C=O)[38]	
1640-1680		ν(C=C)	Amide I[46]
1454, 1444		$\delta(CH_2)$[47]	
1304		$\tau_{ip}(CH_2)$[46]	
1284			Amide III, α helix[39]
1271		δ(=C-H)[46]	
1250, 1247			Amide III, unordered, β sheet[39]
1131		ν(C-C)[47]	
1075	$\nu_1(CO_3^{2-})$[42]		
1009			Phe[46]
964	$\nu_1(PO_4^{3-})$ hydroxyapatite[40]		
860			ν(C-C) Pro[48]
704		cholesterol[3,38]	
591	$\nu_4(PO_4^{3-})$[40]		
548		cholesterol[3,7]	
532			ν(S-S)[48]
432	$\nu_2(PO_4^{3-})$[40]		
428		cholesterol[3,7]	

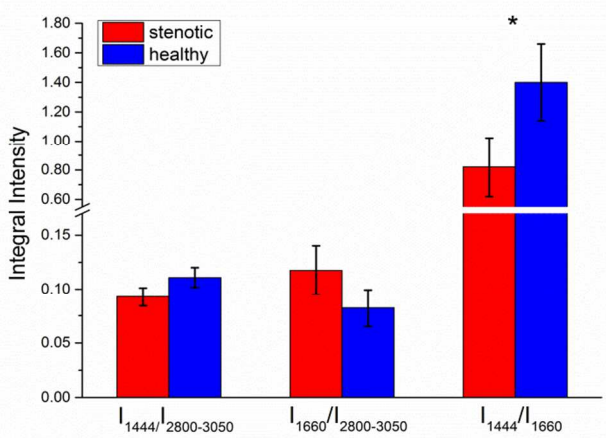

Fig. 2. The ratios of integral intensity of bands at *ca.* 1444 to bands in the range of 2800-3050 cm^{-1}, 1660 to 2800-3050 cm^{-1} and 1444 to 1660 cm^{-1} calculated for the average spectra of stenotic (red) and control (blue) valves (*$p<0.05$).

The comparison of values obtained for stenotic and healthy valves reveals a decrease in the intensity of the band at *ca.* 1444 cm^{-1} relatively to the features at 1660 and in the 2800-3050 cm^{-1} range for stenotic valves. The band at 1444 cm^{-1} is assigned to the vibrations of methylene groups in alkyl chains for both lipids and proteins, however, the first ones have greater

contribution due to the considerably higher number of such groups in the structure. Hence, the lowering of the $I_{1444}/I_{2800-3050}$ ratio indicates the decrease of fatty acids and triacylglycerols content in the tissue relatively to other biocomponents. Besides, the position of this band (1444 cm^{-1} in the control valves) in the spectrum of the stenotic valves (Fig. 1C) is observed at the higher wavenumber, 1454 cm^{-1}, which is more protein-like.[39] The increase of the ratio of the band at 1660 to the band in the 2800-3050 cm^{-1} range shows the relative increase of unsaturated lipids content in stenotic valves in agreement with the relative growth of the band at 1670 cm^{-1} assigned to C=C stretching vibrations.

Statistically, only the ratio 1444/1660 is significantly different ($p<0.05$). Overall, the results show the global increase of cholesterol and its esters with the simultaneous decrease of other lipid components relatively to proteins.

Calcification

The stenotic aortic valve is characterized by the presence of inorganic phosphate salts in the tissue. Fig. 1B shows a representative average spectrum extracted from the dataset with the high salt content. The fingerprint region is dominated by the sharp and intense band at 964 cm^{-1} originating from the P-O stretching vibrations of the phosphate anion (ν_1 PO_4^{3-}) in hydroxyapatite.[40] The position of this band depends on the arrangement of ions in the crystal lattice.[41] It has been shown that in the course of the disease progression the salt structure undergoes various alterations before constituting the final stable form of hydroxyapatite ($Ca_{10}(PO_4)_6(OH)_2$).[33] In the spectrum of the high salt content the hydroxyapatite in a predominant component of deposits as demonstrated also by the position of others bands due to the PO_4^{3-} moiety at 591 (ν_4) and 430 (ν_2) cm^{-1}.[42] Additionally, during the maturation process of crystals some inclusions of other ions i.e. carbonates may occur.[43] The substitution of the OH^- or PO_4^{3-} anions leads to A-type or B-type carbonate, respectively.[41] The position of the carbonate feature is different for both forms. For the A-type carbonated apatite is seen at 1103 cm^{-1}, while for the B-type it is downshifted to 1075 cm^{-1}.[44,45] Thus, the feature at 1075 cm^{-1} seen in the spectrum corresponds to the B-type carbonate substitution.

In spectrum 1C, bands originating from phosphate salts are clearly seen and together with cholesterol are considered spectral markers of global changes in the aortic stenosis (Table 1).

Distribution of biomolecules in tissue

Raman imaging of the valve tissue provides an insight into the biochemical composition and its distribution at the subcellular level. Fig. 3 shows the reflected light images showing areas of two representative measurements and Raman images of major components based on the integration of the characteristic marker bands. The analysis was focused on calcium salts and various lipids.

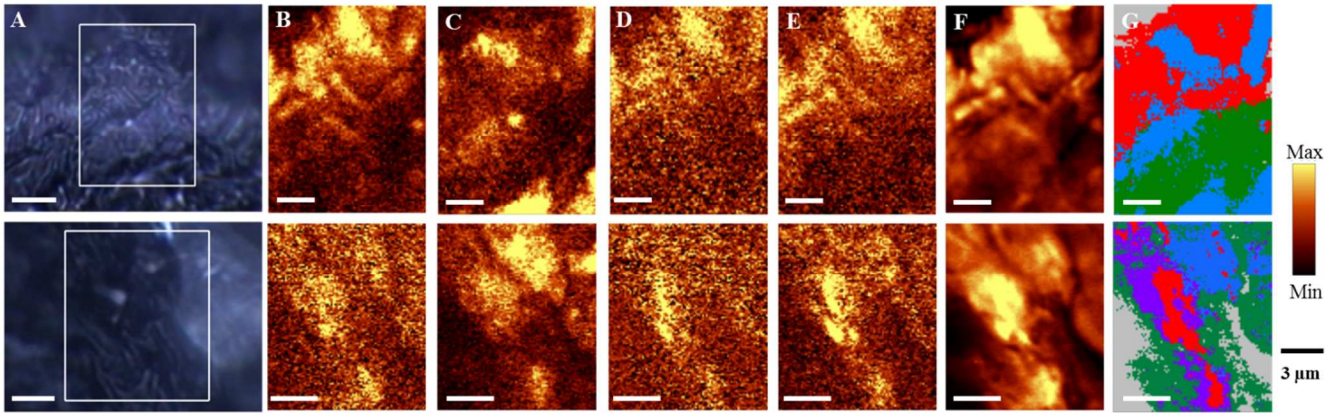

Fig. 3. The representative images of the stenotic valves: the reflected light images of a valve tissue at 100x magnification (A) and Raman distribution images of lipid components obtained by integration of suitable marker bands: cholesterol (B, 704 cm^{-1}), hydroxyapatite (C, 965 cm^{-1}), fatty acid chains (D, 1131 cm^{-1}), esters (E, 1740 cm^{-1}) and lipids (F, 2830-2900 cm^{-1}) for stenotic valves. Yellow color denotes a high concentration of the studied species. The respective cluster map (G, 4 or 5 classes, Manhattan distance) with differentiation into lipids (red and violet area), calcium salts (blue) and other components of the tissue (green).

Fig. 3B-F present images showing distribution of cholesterol, hydroxyapatite, fatty acids chains and esters integrated over the bands at 704, 965, 1131 and 1740 cm^{-1}, respectively. The image in Fig. 3F was obtained by integration of the features in the 2830-2900 cm^{-1} range, mainly related to lipid components present in the tissue. Additionally, staining specific for lipids revealed their abundant accumulation in the neighborhood of calcium deposits at the aortic side of the stenotic leaflets in contrast to healthy ones. However, lipid deposits were also observed in areas without visible calcification (Fig S1, Supplementary Materials).

Apart from the visualization of lipids and hydroxyapatite distribution in stenotic valves, the recorded Raman hyperspectral data enable also discrimination between different

lipids. Overall, lipid composition is dominated by cholesterol and its esters (Fig. 3B and E), with minor addition of triacylglycerols and fatty acids (distinction between images 3D and 3E). Moreover, cholesterol and cholesteryl esters occur as shapeless deposits, contrarily to what was observed in arteries in the murine model of atherosclerosis, where cholesterol exists frequently in the form of well-shaped crystals.[36]

Although distribution of phosphate salts is significantly different than lipids, the comparison of distribution images (3C and 3F) shows that these components are present in the close vicinity. Statistically, in one quarter of the analyzed images calcium salts are accompanied by lipid deposits.

The chemometric approach was applied to analyze obtained data in details. K-means Cluster Analysis (CA) with Manhattan distance was used to separate information about biocomponents in the tissue. The examples of cluster images are presented in Fig. 3G. Implementation of CA enabled to distinguish clearly areas of the high concentration of lipids (red and violet) in the neighborhood of calcium deposits (blue). However, some weak bands originating from lipids were still observed in the average spectra for other clusters (data not shown). It indicates a significant fat degeneration of the aortic valve tissue. The average spectra of lipid classes extracted from the Cluster Analysis images were averaged in order to obtain the representative Raman profile of the lipid deposits. The resulting spectrum was compared with analytical standards from various groups of lipids (Fig. 4A-E).

The Raman spectrum of the averaged lipid class (4F) exhibits characteristic bands at 428 and 704 cm^{-1}, assigned to the sterol ring deformations. Additionally, the low-wavenumber components of the C-H stretching vibrations band indicate a high content of cholesterol. A quite broad band at 1738 cm^{-1} indicates the presence of cholesterol esters, but does not exclude the presence of triacylglycerols that exhibit two bands at 1730 and 1745 cm^{-1}. The unsaturated lipid are also observed due to the presence of the band at 1263 cm^{-1}, quite narrow signal at 1670 cm^{-1} and shoulder at *ca.* 3010 cm^{-1}. Overall, Raman lipid profile is dominated by cholesterol and cholesteryl esters with a possible minor contribution of triacylglycerols. The comparison of spectrum of averaged lipid classes with analytical standards shows that cholesteryl linoleate may be an abundant lipid in the stenotic valve tissue (compare Fig. 4E and 4F).

Additionally, in one exceptional case, Raman image shows a deposit in the form of practically pure lipid (integration over the band at 1300 cm^{-1}, Fig. 5).

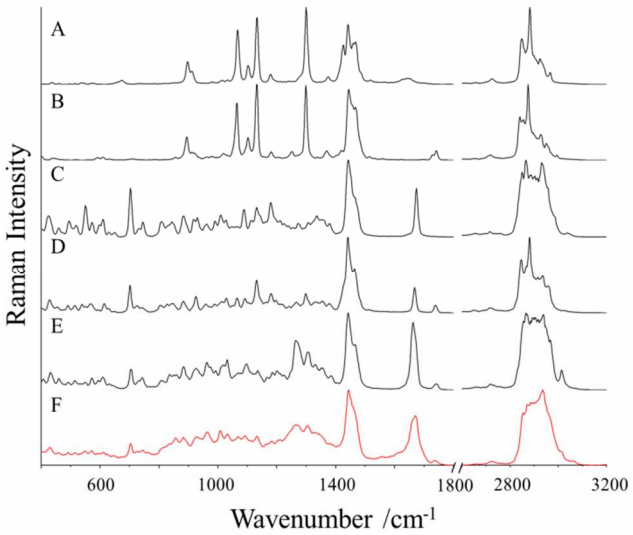

Fig. 4. Comparison of Raman spectra of lipids' standards: A – palmitic acid, B - tripalmitin, C - cholesterol, D – cholesteryl palmitate, E – cholesteryl linoleate with the spectrum of lipid classes extracted from the Cluster Analysis images averaged over all measurements (F). Both spectral ranges were maximally extended in the y-axis.

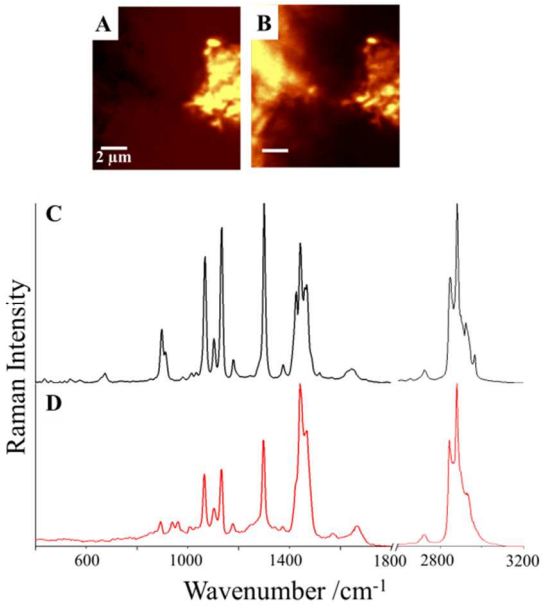

Fig. 5. Distribution images of fatty acids (A) and organic components (B) obtained by integration of bands at *ca.* 1300 cm^{-1} and in the 2830-3040 cm^{-1} range, respectively. The average Raman spectrum for palmitic acid standard (C) and for fatty acid cluster in A (D). Both spectral ranges were maximally extended in the y-axis.

The composition of this deposit was investigated in details by comparing its spectrum with the spectra of analytical standards showing that this deposit is composed of palmitate derivatives, mostly the free acid and its glycerol ester. The accumulation of palmitic acid may have two causes. Firstly, it is one of the most widespread fatty acids, ubiquitous in food products. On the other hand, palmitic acid elevates the activity of oxidized LDL receptor-1 (LOX-1) that is responsible for the uptake of oxidized LDLs.[49] Furthermore, it enhances oxidized LDL uptake in macrophages, promoting them to foam cells formation. This two things, accumulation of oxLDL and alteration of macrophages are important steps initiating atherosclerosis, as well as aortic stenosis.[14,50]

As mentioned above, the structure of calcium deposits changes during development of the valve pathology. Fig. 6 illustrates distribution of cholesterol (A) and phosphate salts (B and C) in the tissue areas with calcification at the early stages of formation.

In contrast to the image presented in Fig. 3, here, calcium salts occur as circular grains with different sizes. The smaller ones (of diameter *ca.* 1 µm) possess significantly different Raman profile with the most intense band at 975 cm^{-1}. The other bands originating from inorganic salts are at 433, 591 and 1076 cm^{-1}. In our previous work[33] we assigned these bands to mixture of β-tricalcium and octacalcium phosphates with carbonate inclusions and classified as the medium stage of mineralization process, while the Raman spectrum of bigger grains (> 2 µm) corresponds to hydroxyapatite structure.

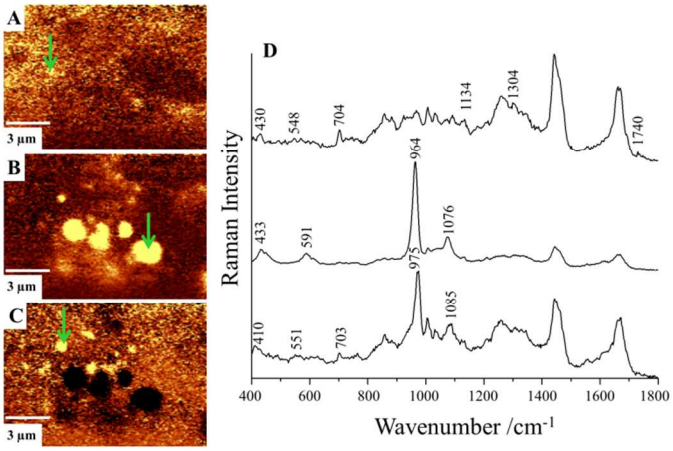

Fig. 6. Raman images of tissue components obtained by integration of the marker bands: 705 cm^{-1} of cholesterol (A), 966 cm^{-1} of hydroxyapatite (B), 975 cm^{-1} of octacalcium phosphate (C) with the corresponding single spectra (D, green arrows shows the voxels from which the spectra were extracted).

Therefore, lipids, primarily cholesterol and its esters (due to bands at 704 and 1740 cm^{-1}, respectively, Fig. 6A), are surrounding also very small inclusions of newly-forming calcific deposits suggesting that cholesterol have an impact on mineralization development, and, therefore, on progression of the aortic stenosis.

Conclusions

As the continuation of our previous study of calcification in the stenotic aortic valves[33], we investigated the biochemical tissue alterations associated with the development of aortic stenosis using Raman microimaging. The particular attention was devoted to the areas in the vicinity of calcification. Statistically, in one quarter of the analyzed images calcium salts were accompanied by lipid deposits. These lipid deposits are composed mainly of cholesterol and its unsaturated esters. Also very small calcium salt grains, at the early stages of mineralization, are surrounded by cholesterol, suggesting that it has an impact on mineralization development.

Overall, the cholesterol level increases in the stenotic valves what can be regarded as a typical hallmark of the development of aortic stenosis next to calcification. Surprisingly, in the average spectra of the stenotic valves, the relative lipid-to-protein ratio decreases. It shows that although cholesterol and its esters content increases in the stenotic valve tissue, the decrease of other lipid components (fatty acids and triacylglycerols) content relatively to proteins takes place. These changes may be related with the process of collagen and elastin remodelling occurring during the pathology development.[51] Overall, Raman microimaging enables recognition and characterization of the biochemical changes occurring in human aortic valves upon aortic stenosis progress.

Acknowledgements

This work was supported by the European Union under the European Regional Development Fund (grant coordinated by JCET-UJ, POIG.01.01.02-00-069/09) and National Science Centre (DEC-2013/08/A/ST4/00308). KC thanks the Krakow Scientific Marian Smoluchowski Consortium "Matter - Energy - Future" for financial support.

Notes and references

[a] Faculty of Chemistry, Jagiellonian University, Ingardena 3, 30-060 Krakow, Poland.
[b] Jagiellonian Centre for Experimental Therapeutics (JCET), Bobrzynskiego 14, 30-348 Krakow, Poland.
[c] Institute of Cardiology, Jagiellonian University, Pradnicka 80, 31-202 Krakow, Poland.
[d] John Paul II Hospital, Pradnicka 80, 31-202 Krakow, Poland

1. F. J. Schoen, *Cardiovasc. Pathol.*, **14**, 189–94.
2. M. S. Sacks, W. David Merryman, and D. E. Schmidt, *J. Biomech.*, 2009, **42**, 1804–24.
3. M. Misfeld and H. H. Sievers, *Philos. Trans. R. Soc. Lond. B. Biol. Sci.*, 2007, **362**, 1421–36.
4. E. H. Stephens, C.-K. Chu, and K. J. Grande-Allen, *Acta Biomater.*, 2008, **4**, 1148–60.
5. P. F. Davies, A. G. Passerini, and C. A. Simmons, *Arterioscler. Thromb. Vasc. Biol.*, 2004, **24**, 1331–3.
6. C. A. Simmons, *J. Am. Coll. Cardiol.*, 2009, **53**, 1456–8.
7. M. R. Dweck, N. A. Boon, and D. E. Newby, *J. Am. Coll. Cardiol.*, 2012, **60**, 1854–63.
8. J. D. Hutcheson, E. Aikawa, and W. D. Merryman, *Nat. Rev. Cardiol.*, 2014, **11**, 218–31.
9. E. Yetkin and J. Waltenberger, *Int. J. Cardiol.*, 2009, **135**, 4–13.
10. A. Parolari, C. Loardi, L. Mussoni, L. Cavallotti, M. Camera, P. Biglioli, E. Tremoli, and F. Alamanni, *Eur. J. Cardiothorac. Surg.*, 2009, **35**, 493–504.
11. E. R. Mohler, *Lancet*, 2000, **356**, 524–5.
12. A. Martinsson, G. Östling, M. Persson, K. Sundquist, C. Andersson, O. Melander, G. Engström, B. Hedblad, and J. G. Smith, *Arterioscler. Thromb. Vasc. Biol.*, 2014, **34**, 2343–8.
13. N. M. Rajamannan, *Am. J. Physiol. Heart Circ. Physiol.*, 2010, **298**, H5–15.
14. E. R. Mohler, *Am. J. Cardiol.*, 2004, **94**, 1396–402, A6.
15. K. D. O'Brien, D. D. Reichenbach, S. M. Marcovina, J. Kuusisto, C. E. Alpers, and C. M. Otto, *Arterioscler. Thromb. Vasc. Biol.*, 1996, **16**, 523–32.

16. M. Olsson, J. Thyberg, and J. Nilsson, *Arterioscler. Thromb. Vasc. Biol.*, 1999, **19**, 1218–22.
17. S. Sarig, T. A. Weiss, I. Katz, F. Kahana, R. Azoury, E. Okon, and H. S. Kruth, *Lab. Invest.*, 1994, **71**, 782–7.
18. M. C. Chui, D. E. Newby, M. Panarelli, P. Bloomfield, and N. A. Boon, *Clin. Cardiol.*, 2001, **24**, 52–5.
19. E. R. Mohler, F. Gannon, C. Reynolds, R. Zimmerman, M. G. Keane, and F. S. Kaplan, *Circulation*, 2001, **103**, 1522–8.
20. K. D. O'Brien, J. Kuusisto, D. D. Reichenbach, M. Ferguson, C. Giachelli, C. E. Alpers, and C. M. Otto, *Circulation*, 1995, **92**, 2163–2168.
21. M. Pilarczyk, A. Rygula, A. Kaczor, L. Mateuszuk, E. Maślak, S. Chlopicki, and M. Baranska, *Vib. Spectrosc.*, 2014, **75**, 39–44.
22. P. P. Kundu and C. Narayana, *J. Med. Allied Sci.*, 2012, **2**, 41–48.
23. K. Majzner, A. Kaczor, N. Kachamakova-Trojanowska, A. Fedorowicz, S. Chlopicki, and M. Baranska, *Analyst*, 2013, **138**, 603–10.
24. B. Singh, R. Gautam, S. Kumar, V. B. Kumar, U. Nongthomba, D. Nandi, G. Mukherjee, V. Santosh, K. Somasundaram, and S. Umapathy, *Curr. Sci.*, 2012, **102**, 232.
25. K. R. McNaughton, D., Wood, B.R., Cox, T.C., Drenckhahn, J.C., Bambery, in *Infrared and Raman Spectroscopic Imaging*, eds. R. Salzer and H. W. Siesler, Wiley-VCH Verlag GmbH & Co. KGaA, Weinheim, Germany, 2009, pp. 203–220.
26. F. Bonnier, A. Mehmood, P. Knief, A. D. Meade, W. Hornebeck, H. Lambkin, K. Flynn, V. McDonagh, C. Healy, T. C. Lee, F. M. Lyng, and H. J. Byrne, *J. Raman Spectrosc.*, 2011, **42**, 888–896.
27. C. Krafft and V. Sergo, 2006, **20**, 195–218.
28. M. Pilarczyk, L. Mateuszuk, A. Rygula, M. Kepczynski, S. Chlopicki, M. Baranska, and A. Kaczor, *PLoS One*, 2014, **9**, e106065.
29. K. Kochan, K. M. Marzec, K. Chruszcz-Lipska, A. Jasztal, E. Maslak, H. Musiolik, S. Chłopicki, and M. Baranska, *Analyst*, 2013, **138**, 3885–90.
30. H. Nawaz, F. Bonnier, P. Knief, O. Howe, F. Lyng, A. Meade, and H. Byrne, *Evaluation of the Potential of Raman Microspectroscopy for Prediction of Chemotherapeutic Response to Cisplatin in Lung Adenocarcinoma*, 2010.
31. G. V Nogueira, L. Silveira, A. a Martin, R. a Zângaro, M. T. T. Pacheco, M. C. Chavantes, and C. a Pasqualucci, *J. Biomed. Opt.*, 2005, **10**, 031117.
32. J. Kneipp, T. B. Schut, M. Kliffen, M. Menke-Pluijmers, and G. Puppels, *Vib. Spectrosc.*, 2003, **32**, 67–74.
33. M. Pilarczyk, K. Czamara, M. Baranska, J. Natorska, P. Kapusta, A. Undas, and A. Kaczor, *J. Raman Spectrosc.*, 2013, **44**, 1222–1229.
34. K. Banas, A. M. Banas, M. Gajda, W. M. Kwiatek, B. Pawlicki, and M. B. H. Breese, *Radiat. Phys. Chem.*, 2013, **93**, 82–86.
35. S. M. Ali, F. Bonnier, A. Tfayli, H. Lambkin, K. Flynn, V. McDonagh, C. Healy, T. Clive Lee, F. M. Lyng, and H. J. Byrne, *J. Biomed. Opt.*, 2013, **18**, 061202.
36. K. M. Marzec, T. P. Wrobel, A. Rygula, E. Maslak, A. Jasztal, A. Fedorowicz, S. Chlopicki, and M. Baranska, *J. Biophotonics*, 2014.
37. K. Czamara, K. Majzner, M. Pilarczyk, K. Kochan, A. Kaczor, and M. Baranska, *J. Raman Spectrosc.*, 10.1002/jrs.4607.
38. C. Krafft, L. Neudert, T. Simat, and R. Salzer, *Spectrochim. Acta Part A Mol. Biomol. Spectrosc.*, 2005, **61**, 1529–1535.
39. A. Rygula, K. Majzner, K. M. Marzec, A. Kaczor, M. Pilarczyk, and M. Baranska, *J. Raman Spectrosc.*, 2013, **44**, 1061–1076.
40. G. R. Sauer, W. B. Zunic, J. R. Durig, and R. E. Wuthier, *Calcif. Tissue Int.*, 1994, **54**, 414–420.
41. B. Wopenka and J. D. Pasteris, *Mater. Sci. Eng. C*, 2005, **25**, 131–143.
42. A. Antonakos, E. Liarokapis, and T. Leventouri, *Biomaterials*, 2007, **28**, 3043–3054.
43. A. Awonusi, M. D. Morris, and M. M. J. Tecklenburg, *Calcif. Tissue Int.*, 2007, **81**, 46–52.
44. M. Kozielski, T. Buchwald, M. Szybowicz, Z. Błaszczak, A. Piotrowski, and B. Ciesielczyk, *J. Mater. Sci. Mater. Med.*, 2011, **22**, 1653–61.
45. G. Penel, G. Leroy, C. Rey, and E. Bres, *Calcif. Tissue Int.*, 1998, **63**, 475–81.
46. Z. Movasaghi, S. Rehman, and I. U. Rehman, *Appl. Spectrosc. Rev.*, 2007, **42**, 493–541.
47. J. De Gelder, K. De Gussem, P. Vandenabeele, and L. Moens, *J. Raman Spectrosc.*, 2007, **38**, 1133–1147.
48. B. G. Frushour and J. L. Koenig, *Biopolymers*, 1975, **14**, 379–91.
49. J. Ishiyama, R. Taguchi, Y. Akasaka, S. Shibata, M. Ito, M. Nagasawa, and K. Murakami, *J. Lipid Res.*, 2011, **52**, 299–307.
50. R. V Freeman and C. M. Otto, *Circulation*, 2005, **111**, 3316–26.
51. V. Dritsa, K. Pissaridi, E. Koutoulakis, I. Mamarelis, C. Kotoulas, and J. Anastassopoulou, *In Vivo*, **28**, 91–8.